Vorticity matching in superfluid helium

By David C. Samuels

1. Motivation and objectives

Experiments by Van Sciver (1990) and others (Weisend *et al.* (1990), Walstrom *et al.* (1988)) have rekindled interest in investigating high Reynolds number flows using superfluid helium (Craig and Pellam (1957)). In a continuing series of experiments, the flow of helium II through various devices (smooth pipes, corrugated pipes, valves, venturies, turbine flowmeters, and coanda flowmeters for example) has been investigated. In all cases, the measured values (typically, mass flow rates and pressure drops) have been found to be well described by classical relations for high Reynolds number flows. This is unexpected since helium II consists of two interpenetrating fluids; one fluid with nonzero viscosity (the normal fluid) and one with zero viscosity (the superfluid). Only the normal fluid component should directly obey classical relations.

Since the experiments listed above only measure the external behavior of the flow (i.e. pressure drops over devices), there is a great deal of room for interpretation of their results. One possible interpretation is that in turbulent flows the normal fluid and superfluid velocity fields are somehow "locked" together, presumably by the mutual friction force between the superfluid vortex filaments and the normal fluid. We refer to this locking together of the two fluids as "vorticity matching".

Stronger evidence for this theory is found in experiments by Borner and Schmidt (1985) which measured the circulation distribution of both the normal fluid and superfluid in macroscopic vortex rings. They found that the vortex ring circulations in both fluids are equal even at the closest measurable distance from the orifice of the vortex ring generator. The Reynolds numbers for the flow inside the ring generator were 20,000 to 40,000.

The primary objective of the present study is to determine the physics responsible for vorticity matching in helium II flows. Similarly, since we know that not all types of helium II flow show vorticity matching, examining the limits of this matching is also an objective of this study.

We are pursuing this project with numerical simulations of superfluid vortex filaments. Each filament is modeled as a series of N nodes connecting straight vortex segments. The meshing of the filaments is automatically adjusted during the simulation in order to keep an approximately constant ratio of segment length to local radius of curvature, within maximum and minimum curvatures, as the filament grows or decays through the mutual friction force. Provisions are included which reconnect the filament mesh whenever a crossing is detected. The self-induced velocity $\vec{V}_i$ of the filament is calculated by the Biot-Savart law, integrated over all filaments in the fluid. Boundary conditions are met by the method of images. Since the Biot-Savart law is a non-local integral, a straightforward implementation, such

as the one we are using, is an order N^2 process. This limits us to a maximum N of a few thousand, running on a Cray Y-MP. A local approximation to the Biot-Savart law would allow us to use a much larger number of mesh points but would ignore the nonlocal interactions that are most important when the length of vortex filament is large. Accordingly, we use the full Biot-Savart law in the simulations reported here.

The total velocity of a node on the vortex filament (Hall and Vinen (1956)) is give by

$$\frac{d\vec{S}}{dt} = \vec{V}_i + \vec{V}_s + \alpha \hat{S}' \times (\vec{V}_n - \vec{V}_s - \vec{V}_i) \tag{1}$$

where $\vec{S}$ is the position of the node, $\vec{V}_s$ is the superfluid velocity from sources other than the superfluid vortex filaments, $\vec{V}_n$ is the normal fluid velocity field, α is a temperature dependent mutual friction coefficient, and $\hat{S}'$ is the local tangent vector of the filament. The value of α is well known at all temperatures from experiment (Barenghi, Donnelly and Vinen (1983)) and is understood theoretically for temperatures below approximately 1.8 Kelvin (Samuels and Donnelly (1990)). This equation of motion is solved by a Runge-Kutta-Fehlberg method.

2. Accomplishments

The most general accomplishment of this study has been the determination of two necessary conditions for vorticity matching. These conditions are:

a) A one dimensional (or higher) region where $\vec{V}_n = \vec{V}_s$ must initially exist in the fluid.

b) A source of superfluid vorticity must be present.

The region with $\vec{V}_n = \vec{V}_s$ must be at least one dimensional so that a superfluid vortex filament can fit within this region. The normal fluid at the boundary of the matched velocity region will have some vorticity $\vec{\omega}_n$. Superfluid vortex filaments with a component of vorticity in the same direction as $\vec{\omega}_n$ are transported by mutual friction from the superfluid vorticity source to the boundary of the region of matched velocities. As the filaments accumulate here, the superposition of their velocity fields extends the matched velocity region to a larger (three dimensional) volume.

A useful example of a flow which satisfies condition (a) is the normal fluid vortex. Assuming for simplicity that $\vec{V}_n$ is a vortex flow with some core structure and $\vec{V}_s = 0$, on the axis of the normal fluid vortex $\vec{V}_n - \vec{V}_s$ goes to zero, and condition (a) is met. Superfluid vortex filaments with the same orientation of circulation as the normal fluid vortex will be attracted to the normal fluid vortex core by mutual friction, and filaments of the opposite circulation will be repulsed. If some source of superfluid vorticity (condition (b)) exists, then we would expect normal fluid vortices to show vorticity matching. This type of flow is important to our understanding of the vorticity matching of high Reynolds number flows in superfluid helium since it provides a simple model for the interaction of superfluid vortex filaments with concentrated vortex structures in the turbulent normal fluid flow.

In this case, the superfluid vorticity source is provided by the instability of vortex filaments in a background shear. Aref and Flinchem (1984) observed this instability in simulations of vortex solitons with an applied velocity shear but did not correctly identify the cause. Later, Pierrehumbert (1986) identified this behavior as an instability of infinitesimal sinusoidal vortex waves in a background shear. With straightforward modifications to include mutual friction, this instability is applicable to superfluid vortex filaments with external superfluid and normal fluid flow fields. We consider the case where the normal fluid flow is a vortex flow

$$V_{n\theta} = \frac{N_n \kappa}{2\pi r} \tag{2}$$

where N_n is the ratio of the normal fluid circulation to the superfluid circulation quantum κ. We also impose an external superfluid vortex flow field

$$V_{s\theta} = \frac{N_s \kappa}{2\pi r} \tag{3}$$

where N_s is the number of circulation quantums of the field. This external superfluid flow is included to represent the velocity field of any superfluid vortex filaments trapped at the center of the normal fluid vortex. With these external fields, the frequency of sinusoidal waves on a superfluid vortex parallel to the normal fluid vortex is

$$\omega T = i\pi\alpha \left[\frac{2s(N_n - N_s)}{(rk)^2 G} - 1\right] \pm 2\pi \left((1 - \frac{\alpha^2}{4}) + \frac{s2N_s}{(rk)^2 G} - \frac{\alpha^2 (N_n - N_s)^2}{(rk)^4 G^2} + \frac{\alpha^2 (N_n - N_s)}{(rk)^2 G} \right)^{\frac{1}{2}} \tag{4}$$

where T is the wave period at absolute zero temperature, k is the wavenumber, $s = \pm 1$ is the sign of the filament circulation, and $G = \ln(1/ka_o)$ where the filament core size a_o is approximately one Ångstrom. Since the situation considered here is slightly different than that treated by Pierrehumbert (1986), we provide the derivation of equation (4) in the appendix.

For a pure normal fluid vortex ($N_s = 0$), with positive circulation, waves on superfluid vortex filaments with negative circulation are damped at all distances, while waves on positive vortex filaments are unstable within a critical distance r_c given by

$$\frac{r_c}{\lambda} = \left(\frac{N_n}{2\pi^2 G}\right)^{\frac{1}{2}} \tag{5}$$

where $\lambda = 2\pi/k$. The instability of these waves triggers a process of exponential growth of the superfluid vortex filament.

This exponential growth process is illustrated by the simulation results shown in figures 1 and 2. This simulation was run with a normal fluid vortex of strength

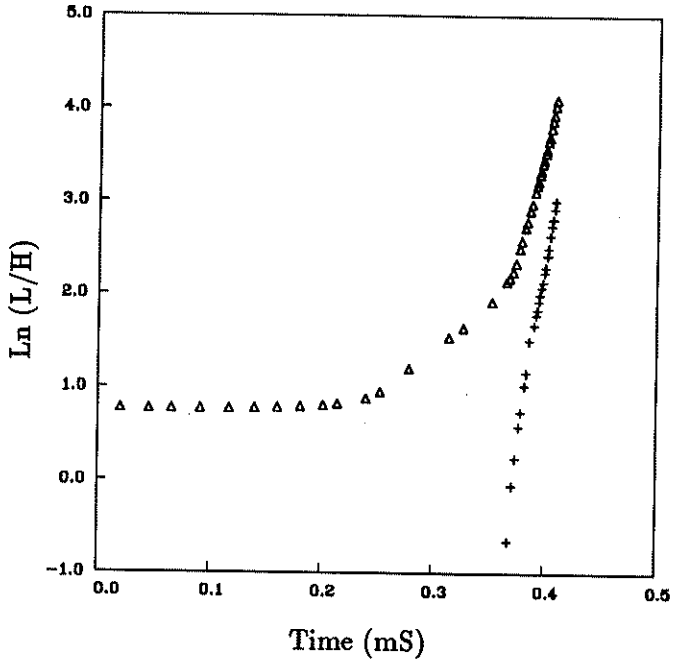

FIGURE 1. Vortex filament length vs. time. (△) denotes the total length of superfluid vortex filament. (+) denotes the length of superfluid vortex filament present inside the normal fluid vortex core.

$N_n = 1000$ along the Z axis. The core size of the normal fluid vortex was set at $R_{core} = .01H$, where H is the height of the computational box, and the interior of the normal fluid vortex core was modeled as solid body rotation. The temperature was $T = 1.6K$, where $\alpha = .16$. The initial conditions were two superfluid vortex filaments, one with positive circulation relative to the normal fluid vortex and the other with negative circulation (figure 2a). Each vortex filament carried a sinusoidal wave with wavelength $\lambda = H/4$. In order to decrease the computational time, the initial amplitude of the waves was sizeable, $A = .09\lambda$. Each filament was placed on opposite sides of the normal fluid vortex at a distance $r = .47H$ from the origin, within the critical radius $r_c = .54H$. The positive circulation filament is attracted to the normal fluid vortex, and its wave grows in amplitude. The negative circulation filament is slowly repulsed from the normal fluid vortex, and its wave decreases in amplitude. Simulations conducted with the negative vortex filament initially closer to the origin show the same decrease in wave amplitude, confirming that the wave instability is due to the circulation sign and not the closer approach of the positive filament to the normal fluid vortex.

The increase in length of superfluid vortex filament is characterized by three stages, easily seen in figure 1. The first stage is simply the exponential growth of the wave amplitude. This stage ends when the amplitude becomes equal to half the wavelength (figure 2b). In the second stage, the behavior is best described as the

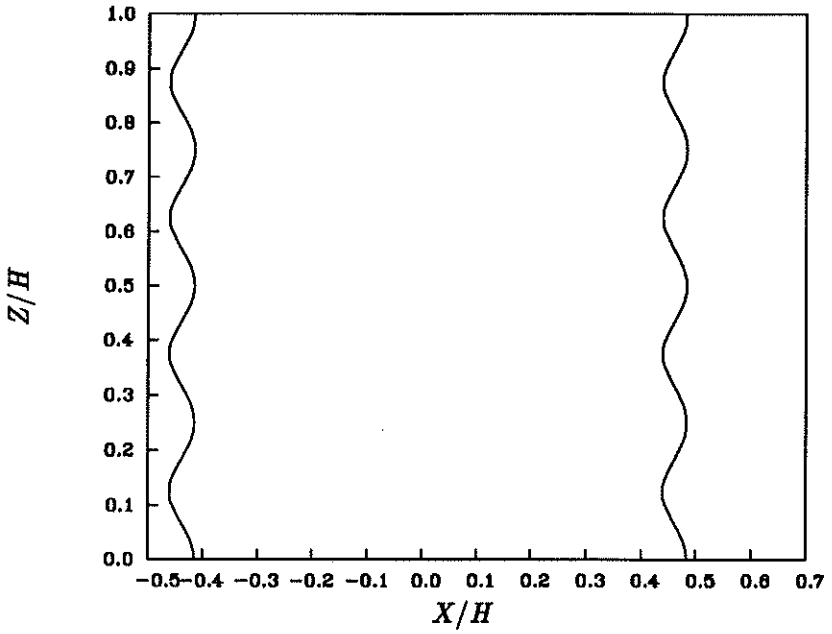

FIGURE 2A. Evolution of the superfluid vortex filaments. $t = .02mS$. The positive filament is on the left.

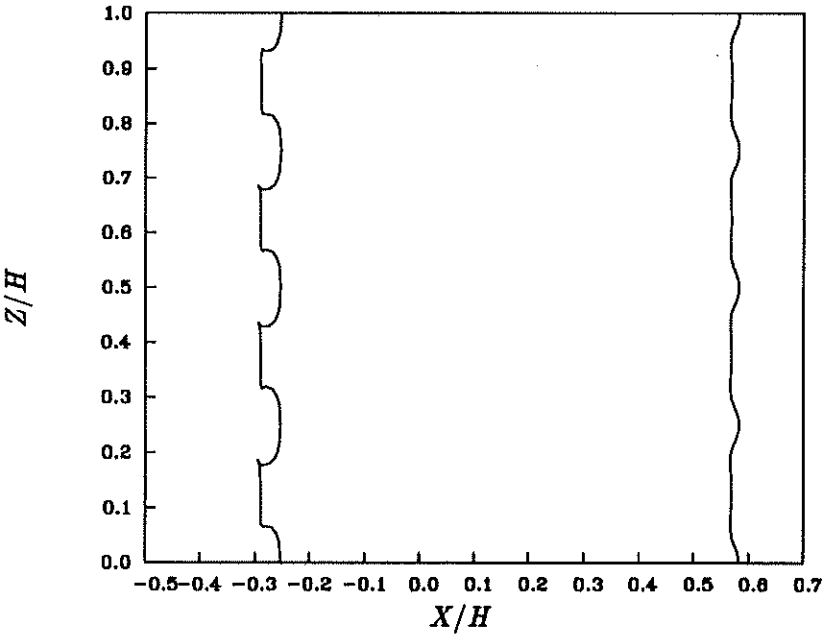

FIGURE 2B. $t = .24mS$.

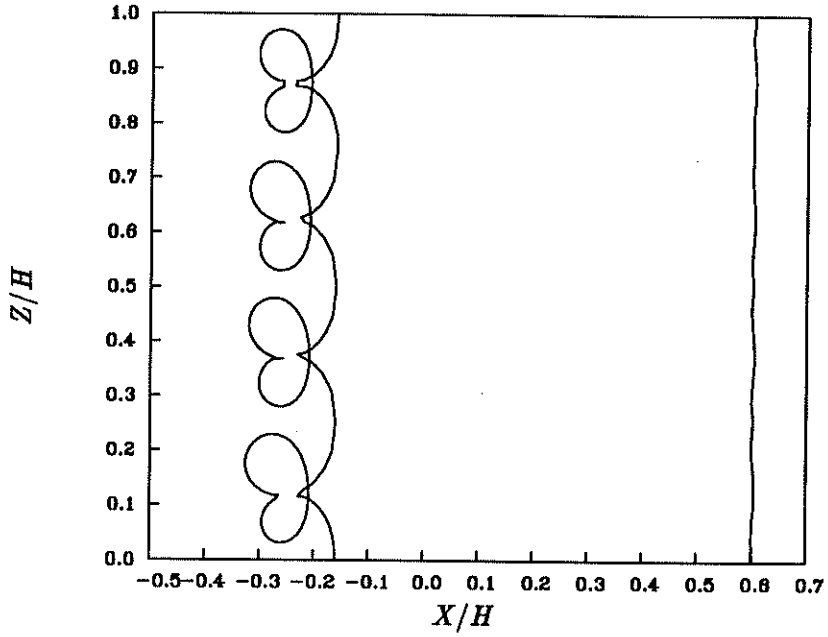

FIGURE 2C. $t = .31mS$.

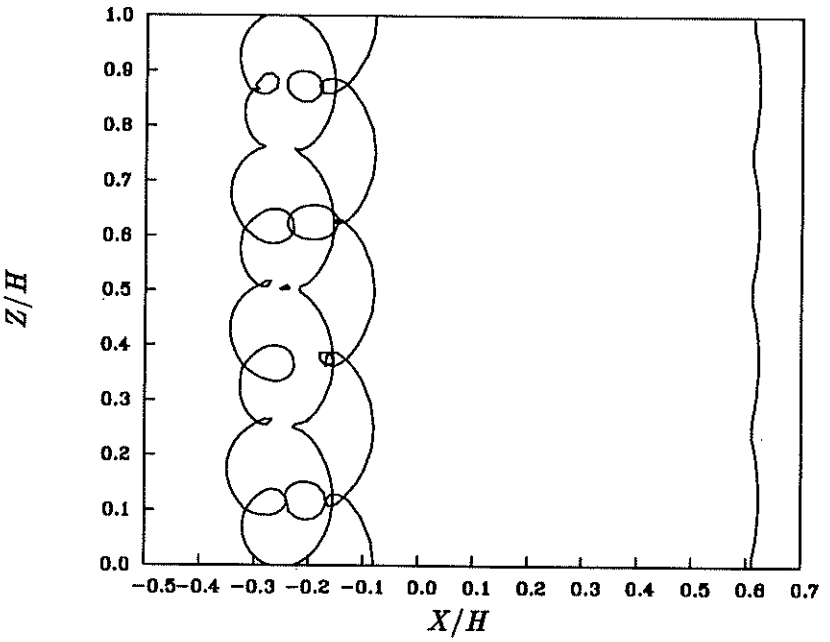

FIGURE 2D. $t = .35mS$.

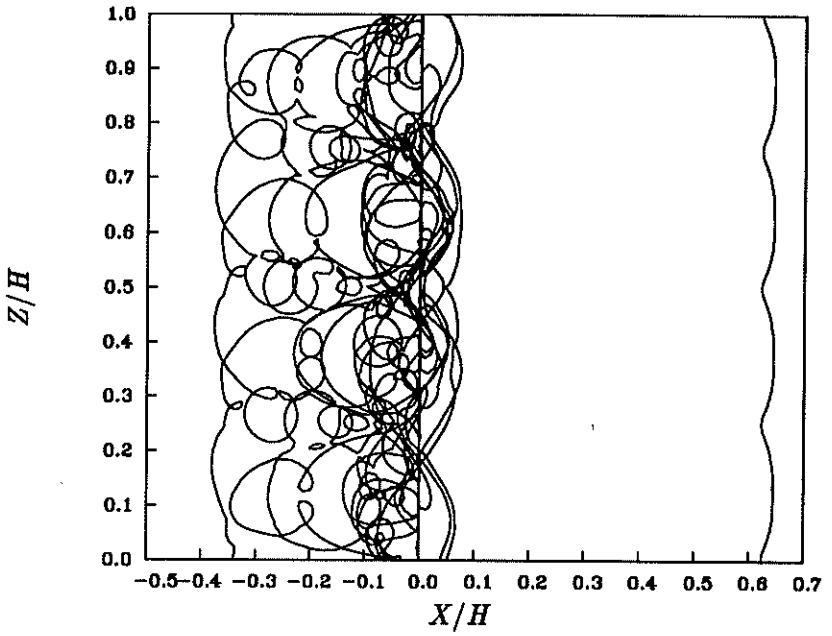

FIGURE 2E. $t = .40mS$.

growth of a series of rings (figure 2c). The growth rate is increased greatly in this stage. During this stage, the rings grow large enough to reconnect, forming new vortex filaments which span the length of the computational volume (figure 2d). The vortex lines continue to "bud" vortex rings, ultimately forming a dense region of interacting superfluid vortex filaments (figure 2e). The third stage is defined by another large increase in the growth rate and by a significant accumulation of vortex filaments inside the normal fluid vortex core (figure 2e and figure 1). The process responsible for this accelerated growth is unknown. It is important for us to understand the time scales for the growth of the superfluid vortex filament since these time scales must be short in comparison to the lifetimes of concentrated vortices in the normal fluid turbulence if there is to be any vorticity matching in a turbulent flow.

It should be emphasized that this vorticity cluster (figure 2e) is quite different from the vortex tangles that develop in simulations of counterflow (Schwarz (1988)) since this vorticity is highly ordered on the large scale, consisting mainly of distorted rings oriented parallel to the normal fluid flow. The degree of order of the vorticity can be quantified in the following manner. The direction of a section of curved vortex filament can be defined by the "binormal" unit vector

$$\hat{b} \equiv \hat{S}' \times \hat{S}'' \tag{6}$$

where $\vec{S}$ is the position vector of the filament and a prime denotes a derivative by arclength. The binormal vector points in the direction of the velocity due to the local curvature of the vortex filament (Arms and Hama (1965), and thus provides a good

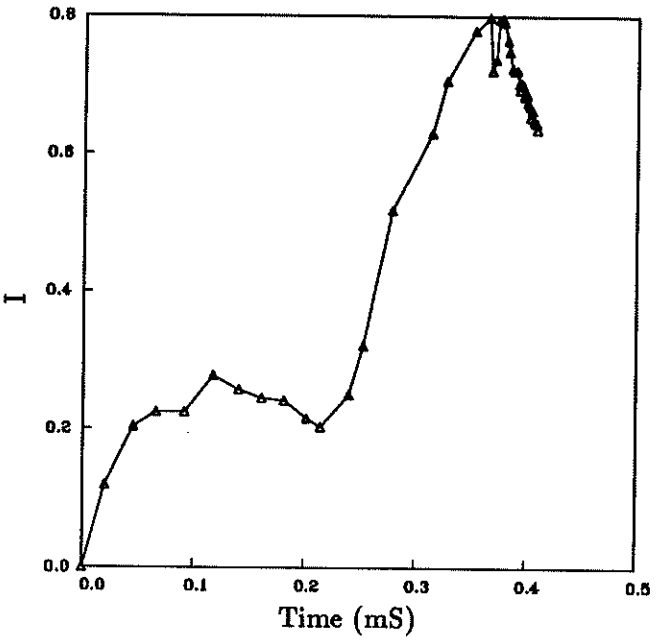

FIGURE 3A. Correlation of binormal vector with normal fluid velocity averaged over all vortex filaments outside the normal fluid core.

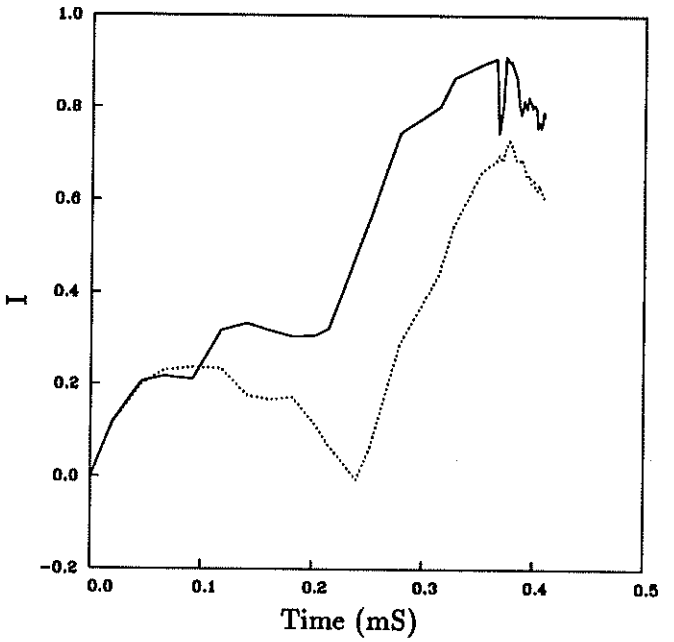

FIGURE 3B. Correlation of binormal vector with normal fluid velocity averaged separately over positive circulation filaments (solid line) and negative (dotted line).

indicator of how the curvature of the vortex filament is reacting to an externally applied velocity field. Take a line integral

$$I = \frac{\int \hat{b} \cdot \hat{v} d\vec{S}}{\int d\vec{S}} \tag{7}$$

where $\hat{v}$ is some reference unit vector. This integral measures the correlation of the binormal and the reference vector. For the geometry of this simulation, we take the reference vector to be the azimuthal unit vector, which is the direction vector of the normal fluid flow. Since the vortex filaments inside the normal fluid vortex core are extremely straight, their binormals are undefined (they have no "direction"). With this in mind, the line integral is restricted to filaments outside the core radius. In figure 3a, we show the results of this calculation. The vortex filaments, initially uncorrelated with the normal fluid flow, become very highly correlated, reaching a maximum correlation of .8 averaged over all the filaments. When positive and negative circulation vortex segments (defined by the sign of the Z component of the tangent vector of each segment) are considered separately, both signs of vorticity show some correlation, with the positive circulation correlation significantly higher than that for the negative circulation (figure 3b).

The end of the first stage gives us a limitation on the minimum strength N_n of the normal fluid vortex which can follow the procedure described above. In order for the wave amplitude to reach $\lambda/2$, the distance of the superfluid vortex filament from the core of the normal fluid vortex must be greater than $\lambda/2$. Inside the core of the normal fluid vortex, the superfluid vortex wave is damped, and the superfluid vortex filament quickly straightens. If we write the critical radius r_c as

$$r_c > \frac{\lambda}{2} + R_{core} \tag{8}$$

we can derive a minimum N_n from equation (5).

$$N_n > 2\pi^2 G \left(\frac{1}{2} + \frac{R_{core}}{\lambda} \right) \tag{9}$$

Since G is a very slowly changing logarithmic function, we can approximate it by $G = 15 \pm 5$ over many orders of magnitude in λ. By also assuming that $\lambda \gg R_{core}$, we can write equation (9) as

$$N_n > 75 \pm 25 \tag{10}$$

This number should be considered only a lower limit on the actual smallest unstable N_n.

3. Future plans

(1) Determine the role of the normal fluid vortex core in the matching process. This may be an important part of the rapid growth phase.

(2) Attempt to follow the vorticity matching process to completion. We cannot do this directly, but with a greater understanding of the behavior of superfluid vortex filaments inside the normal fluid vortex core, we may be able to form a simple model of their effect on the superfluid vorticity outside the core.

(3) Closely examine the ring budding behavior seen in figure 2d. We must establish that this process is not a numerical artifact.

(4) Determine the time scales of the superfluid filament growth and compare them to the time scales of the normal fluid turbulence.

(5) Consider the reaction of the normal fluid to the superfluid vortices. In all simulations of superfluid vortices, the normal fluid velocity field is considered to be an input to the program. We cannot calculate in detail the response of the normal fluid, but we may be able to include the energy transfer between the fluids in some average manner.

(6) Examine the motion of matched superfluid - normal fluid vortices. Will motion of the matched vortices cause some decoupling of the vorticities?

(7) Simulate the vorticity matching process in the presence of external $\vec{V}_n$ and $\vec{V}_s$. Will external flows interfere with the vorticity matching?

Appendix

Consider a straight vortex filament perturbed by a sinusoidal disturbance.

$$\begin{bmatrix} x \\ y \\ z \end{bmatrix} = \begin{bmatrix} x_0 \\ y_0 \\ z_0 \end{bmatrix} + \begin{bmatrix} \tilde{x} \\ \tilde{y} \\ 0 \end{bmatrix} e^{i(kz-\omega t)} \tag{A1}$$

To conform with the notation of Pierrehumbert (1986), we write the equation of motion (equation (1)) as

$$\frac{d\vec{S}}{dt} = \vec{V}_i + \vec{U} \tag{A2}$$

where we have defined

$$\vec{U} \equiv \vec{V}_s + \alpha \hat{S}' \times (\vec{V}_n - \vec{V}_s - \vec{V}_i). \tag{A3}$$

In the low amplitude limit, the self induced velocity of a sinusoidal vortex wave is

$$\vec{V}_i = s\frac{2\pi}{T} \begin{bmatrix} \tilde{y} \\ -\tilde{x} \\ 0 \end{bmatrix} e^{i(kz-\omega t)} \tag{A4}$$

where $s = \pm 1$ defines the sign of the vortex circulation and T is the period of the undisturbed wave. Applying equation (A2) to equation (A1) yields

$$\begin{bmatrix} dx_0/dt \\ dy_0/dt \end{bmatrix} + \begin{bmatrix} \tilde{x} \\ \tilde{y} \end{bmatrix} (-i\omega) e^{i(kz-\omega t)} = s\frac{2\pi}{T} \begin{bmatrix} \tilde{y} \\ -\tilde{x} \end{bmatrix} e^{i(kz-\omega t)} + \vec{U}. \tag{A5}$$

We are only considering the case where the Z component of $\vec{U}$ is zero. In this case, the Z component of equation (A2) is trivially $dz_0/dt = 0$ and is dropped for the rest of this analysis. Now we linearize $\vec{U}$. We choose to define the X and Y axes so that the gradient of $\vec{U}$ is along the Y axis.

$$\vec{U} \simeq \vec{U}_0 + \left.\frac{d\vec{U}}{dy}\right|_{y_0} e^{i(kz-\omega t)} \tag{A6}$$

For compactness, define

$$\left.\frac{d\vec{U}}{dy}\right|_{y_0} \equiv \begin{bmatrix} U'_x \\ U'_y \end{bmatrix}. \tag{A7}$$

Using the linearized $\vec{U}$ in equation (A5) yields

$$\begin{bmatrix} dx_0/dt \\ dy_0/dt \end{bmatrix} = \vec{U}_0 \tag{A8}$$

and

$$\begin{bmatrix} \tilde{x} \\ \tilde{y} \end{bmatrix} (i\omega) = s\frac{2\pi}{T}\begin{bmatrix} \tilde{y} \\ -\tilde{x} \end{bmatrix} + \begin{bmatrix} U'_x \\ U'_y \end{bmatrix} \tilde{y}. \tag{A9}$$

From equation (A9), we solve for ω.

$$\omega = \tfrac{1}{2} i U'_y \pm \left(s\frac{2\pi}{T}\left(s\frac{2\pi}{T} + U'_x\right) - \tfrac{1}{4} U'^2_y \right)^{\frac{1}{2}} \tag{A10}$$

For the case where the velocity fields $\vec{V}_n$ and $\vec{V}_s$ are vortex flows (equations (2) and (3)), we have

$$U'_x = \frac{N_s \kappa}{2\pi r^2} \tag{A11}$$

and

$$U'_y = \alpha\left(\frac{s(N_n - N_s)\kappa}{2\pi r^2} - \frac{2\pi}{T}\right) \tag{A12}$$

Using equation (A11), equation (A12) and $T = 8\pi^2/\kappa k^2 G$ in equation (A10) yields equation (4).

REFERENCES

AREF, H. & FLINCHEM, E. P. 1984 Dynamics of a vortex filament in a shear flow. *J. Fluid. Mech.* **148**, 477-497.

ARMS, R. J. & HAMA, F. R. 1965 Localized-induction concept on a curved vortex and motion of an elliptic vortex ring. *Phys. Flu.* **8**, 553-559.

BARENGHI, C. F., DONNELLY, R. J., & VINEN, W. F. 1983 Friction on quantized vortices in helium II. A Review. *J. Low Temp. Phys.* **52**, 189-247.

BORNER, H. & SCHMIDT, D. W. 1985 Investigation of large-scale vortex rings in He II by acoustic measurements of circulation. *Lect. N. Phys.* **235**, 135-146.

CRAIG, P. P. & PELLAM, J. R. 1957 Observation of perfect potential flow in superfluid. *Phys. Rev.* **108**, 1109-1112.

HALL, H. E. & VINEN, W. F. 1956 The rotation of liquid helium II. The theory of mutual friction in uniformly rotating helium II. *Proc. Roy. Soc. A.* **210**, 215-234.

PIERREHUMBERT, R. T. 1986 Remarks on a paper by Aref and Flinchem. *J. Fluid. Mech.* **163**, 21-26.

SAMUELS, D. C. & DONNELLY R.J. 1990 Dynamics of the interaction of rotons with quantized vortices in helium II. *Phys. Rev. Lett.* **65**, 187-190.

SCHWARZ, K. W. 1988 Three-dimensional vortex dynamics in superfluid He4: Homogeneous superfluid turbulence. *Phys. Rev. B.* **38**, 2398-2417.

VAN SCIVER, S. W., HOLMES, D. S., HUANG, X., & WEISEND II, J. G. 1991 He II flowmetering. *Cryo.* **31**, 75-86.

WALSTROM, P. L., WEISEND II, J. G., MADDOCKS, J. R., & VAN SCIVER, S. W. 1988 Turbulent flow pressure drop in various He II transfer system components. *Cryo.* **28**, 101-109.

WEISEND II, J. G. & VAN SCIVER, S. W. 1990 Pressure drop from flow of cryogens in corrugated bellows. *Cryo.* **30**, 935-941.